SUPPLEMENTAL MATERIAL

Ballistic transport of long wavelength phonons and thermal conductivity accumulation in nanograined silicon-germanium alloys

Long Chen,[1] Jeffrey L. Braun,[2] Brian F. Donovan,[2,3] Patrick E. Hopkins,[1,2,4,*] and S. Joseph Poon[1,**]

[1] *Department of Physics, University of Virginia, Charlottesville, Virginia 22904-4714, USA*

[2] *Department of Mechanical & Aerospace Engineering, University of Virginia, Charlottesville, Virginia 22904-4746, USA*

[3] *Current Address*: *Department of Physics, United States Naval Academy, Annapolis, Maryland 21402-5002, USA*

[4] *Department of Materials Science and Engineering, University of Virginia, Charlottesville, Virginia 22904-4745, USA*

*phopkins@virginia.edu
**sjp9x@virginia.edu

This supplemental material includes:

S1. Details of the "Fixed Boundary Length" (FBL) and "Spectral Boundary Length" (SBL) models, assumptions and calculations

S2. TDTR Measurements

S3. Validity of the use of a diffusive heat equation-based model when analyzing TDTR data

S4. The cut-off mean free path vs thermal penetration depth determined by the bridge function and hard cutoff approaches

S5. Details of spectral thermal conductivity calculations using the DEM approach for nanograined $Si_{80}Ge_{20}$ systems

S1. Details of the "Fixed Boundary Length" (FBL) and "Spectral Boundary Length" (SBL) models, assumptions and calculations

For the SiGe calculations in this work, we use the model developed for phonon thermal conductivity in SiGe alloys developed by Wang and Mingo[1] and also experimentally validated against SiGe thin films by Cheaito *et al*.[2] The total phonon scattering time is determined by contributions from defect scattering, Umklapp scattering, and grain boundary scattering. These scattering mechanisms are combined using Matthiessen's rule: $\tau_{\mathrm{total}}(\mathrm{q})^{-1} = \tau_{\mathrm{defect}}(\mathrm{q})^{-1} + \tau_{\mathrm{umkl}}(\mathrm{q},\mathrm{T})^{-1} + \tau_{\mathrm{b}}(\mathrm{q})^{-1}$ Each scattering component is modeled as follow:

$$\tau_{\mathrm{defect}}(\mathrm{q})^{-1} = \mathrm{A}\omega^4 \qquad \text{(S1)}$$

$$\tau_{\mathrm{umkl}}(\mathrm{q},\mathrm{T})^{-1} = \mathrm{B}\omega^2 T e^{(-c/T)} \qquad \text{(S2)}$$

$$\tau_{\mathrm{b}}(\mathrm{q})^{-1} = v/l \qquad \text{(S3)}$$

We use the same constants A, B and C in Eqs. (S1) – (S3) that are listed in Wang and Mingo's previous work.[1]

It is important to account for the physical geometry of the structure that creates the boundary that could impede phonon transport. For example, circular boundaries could impact phonon scattering differently than rectangular boundaries. Furthermore, the characteristic structure and properties of the material that is creating the boundaries and structures in a host material must also be accounted for in thermal conductivity calculations (e.g., mass and force constant changes at, for example, a grain or nanoparticle boundary). We can consider boundary scattering, l as the length characteristic of the material defined as $l = (\rho * \sigma)^{-1}$, where ρ is the number of particles in a unit volume which can be determined by $\rho = 6\varphi/\pi \mathrm{R}^3$, where R is the radius of the spherical nanoparticle, and σ is cross section. We can further break down σ as the combination of scattering cross section in two extreme regimes:[3]

$$\sigma_{\mathrm{total}}^{-1} = \sigma_{\mathrm{Ray}}^{-1} + \sigma_{\mathrm{nGeo}}^{-1} \text{ (S4)}$$

Where σ_{Ray} and σ_{nGeo} are scattering cross sections in the Rayleigh limit and near geometric limit, respectively.

Kim and Majumdar proposed an approximate analytical solution to estimate the phonon scattering cross section of polydispersed spherical nanoparticles. They perturbed the Hamiltonian via differences in mass and bond stiffness between a host medium and a spherical nanoparticle for the scattering cross section in the Rayleigh limit, using the van de Hulst approximation for anomalous diffraction in the near geometrical limit.[3]

Based on Kim and Majumdar's work,[3] the scattering cross sections at the Rayleigh limit and near geometrical limit can be expressed as:

$$\sigma_{\mathrm{Ray}} = \pi \mathrm{R}^2 \chi^4 \left(\frac{\beta^2}{4} \left(\frac{\Delta M}{M} \right)^2 + 3\beta^8 \left(\frac{\Delta K}{K} \right)^2 \frac{\left(\sin\frac{\beta|\vec{q}|\delta}{2}\right)^4}{\left(\frac{\beta|\vec{q}|\delta}{2}\right)^4} \right) \frac{\pi(\cos(4\chi) - 1 + (4\chi)\sin(4\chi) + 32\chi^4 - 8\chi^2)}{16\chi^6} \qquad \text{(S5)}$$

$$\sigma_{Geo} = 2\pi R^2\left(1 - \frac{\sin\left(2\chi\left(\frac{q'}{q}-1\right)\right)}{\chi\left(\frac{q'}{q}-1\right)} + \frac{\left(\sin\left(\chi\left(\frac{q'}{q}-1\right)\right)\right)^2}{\left(\chi\left(\frac{q'}{q}-1\right)\right)^2}\right) \quad \text{(S6)}$$

Where χ is the size parameter, defined as $\chi = qR$, where q is the incoming wave vector, q' is the scattered wave vector, δ is the volume size, and β is the polar angle; M and ΔM are the mass of the host and the mass difference between the host and the spherical nanoparticle; K and ΔK denote the force constant of the host medium and the force constant difference between the host and the spherical nanoparticle. The values which we used in the calculation are $\Delta M/M = 0.326$, and $\Delta K/K = 0.131$ by considering the grain distribution.

To take the grain size dispersion into account, the effective scattering cross section was calculated with a normalized grain distribution function F(x):[4]

$$\sigma_{eff} = \int_{d_{min}}^{d_{max}} \sigma_{total}(x)F(x)dx \quad \text{(S7)}$$

where σ_{eff} is the effective scattering cross section, $\sigma_{total}(x)$ is the total scattering section, d_{max} and d_{min} are the upper limit and the lower limit of grain size, and F(x) is the normalized Gamma distribution defined as $F(x) = x^{a-1}\exp[-x/b]/b^a\Gamma(a)$, with the shape parameter a, and scale parameter b, which can be determined by fitting the grain size distribution. The parameters (a, b) are found to be (23.5, 0.085), (5.5, 0.2) and (18.25, 0.4) for $Si_{80}Ge_{20}$ 2.0 ± 0.17 μm, $Si_{80}Ge_{20}$ 110 ± 21 nm, and $Si_{80}Ge_{20}$ 73 ± 29 nm, respectively.

S2. TDTR Measurements

We measure the thermal conductivity of the silicon control sample and the $Si_{80}Ge_{20}$ samples with time domain thermoreflectance.[5-8] Time domain thermoreflectance (TDTR) utilizes a train of ultra-fast laser pulses to thermally stimulate a material system, and a time delayed probe pulse to measure the change in thermoreflectance due to the decay and modulation of the thermal energy deposited by the pump pulse train. This work utilizes sub-picosecond laser pulses emanating from a Ti:Sapph laser system at 80 MHz. The probe pulses are monitored via lock-in detection at the pump modulation frequency for up to 5.5 ns using a mechanical delay stage. We deposit a nominally 80 nm thin film of Al on the sample surface to act as a thermal transducer. We fit a thermal model based on the solution to the radially symmetric heat diffusion equation to the measured decay to determine the thermal conductivity of the Si or $Si_{80}Ge_{20}$ samples. We assume literature values for the other physical properties included in the thermal model including the heat capacity of Si, $Si_{80}Ge_{20}$, and Al,[9,10] which were assumed as 1.64, 1.65, and 2.43 J cm^{-3} K^{-1}, respectively. We assume a reduced thermal conductivity of the Al film based on electrical resistivity measurements and the Wiedemann-Franz law (calculated as 130 W m^{-1} K^{-1}), though we are insensitive to this parameter in our experiment due to our spot sizes and pump-probe delay. We also treat the thermal boundary conductance for the Al/Si or Al/$Si_{80}Ge_{20}$ interface as a free parameter in our model fit. The analysis methods are described in greater detail elsewhere.[5-8] Reported error in the thermal conductivity measurement arises from small thickness variation of the Al transducer and measurement of a number of different sites on the surface of each sample. Using laser spot sizes of 50 μm and 17 μm $1/e^2$ diameters for the pump and probe, respectively, allows us to assume nearly one dimensional heat transfer in the through-plane direction.[8] The bulk Si control sample thermal conductivity was measured to be 135 ± 20 W m^{-1} K^{-1} and independent of modulation frequency.

S3. Validity of the use of a diffusive heat equation-based model when analyzing TDTR data

Wilson and Cahill[11] have questioned the validity of assuming a diffusive heat equation in analyzing TDTR data when frequency dependence in the thermal conductivity is observed. More specifically, as diffusion assumes that a local temperature can be defined, if too many phonons are "escaping" the TDTR measurement volume defined from the spot size and L_z, then the majority of the phonons that define the heat capacity of the solid would not contribute to the measured temperature change, and thus these quantities (heat capacity and temperature) are ill-defined based on literature parameters. They note that to use traditionally implemented TDTR heat diffusion models to analyze the experimental data, the majority of the phononic system that contributes to heat capacity must experience a diffusive scattering event in the measurement volume (i.e., phonons with $q > 0.1q_{\max}$, where for Si, for example, $q_{\max} = 2\pi/\mathrm{a}$).[11] This type of transport would take place in a crystalline alloy, and lead to the frequency dependence in TDTR-measured thermal conductivity, since the majority of the heat conduction is driven by the long wavelength phonons due to the scattering of short wave vector, high frequency phonons with mass impurities.[2,12-15] In other words, in the TDTR measurements presented in this work, the Fourier law does not fail in the analysis of any of these samples.

Similar to the observation of a pump modulation frequency dependent thermal boundary conductance observed by Wilson and Cahill,[11] we also observe this dependence in our bulk $Si_{80}Ge_{20}$ samples. These data are presented in Fig. S1, on (left) semi-log and (right) log-log scales. While this frequency dependence is relatively modest, the trend is consistent with that observed by Wilson and Cahill[11] and suggests that ballistic phonon transport is contributing to the measured thermal boundary conductance (stated differently, phonons are traveling ballistically within some Kapitza length around the Al/$Si_{80}Ge_{20}$ interface). We note the thermal boundary conductances that we measure at these Al/$Si_{80}Ge_{20}$ interfaces are lower than those reported for Al/$Si_{80}Ge_{20}$ interfaces by Wilson and Cahill.[11] This is not surprising since our $Si_{80}Ge_{20}$ samples are bulk and the surface roughnesses are presumably larger than the surface roughnesses in the $Si_{20}Ge_{80}$ samples reported in the work by Wilson and Cahill[11] (albeit surface roughness was not reported in their work, and thus may not have been an issue or as large as our samples studied here). Furthermore, we do not currently understand the differences in thermal boundary conductances that we measure with average grain size variation, but again, surface morphology is well known to affect thermal boundary conductance,[6] and the randomness of the RMS surface roughnesses among the samples along with differing grain size distributions could certainly be playing a role. Regardless, the ability to separate the frequency dependent thermal boundary conductance from the frequency dependent thermal conductivity is a power of using TDTR over FDTR at a fixed delay time or FDTR using continuous wave laser sources, and allows for accurate reporting of the thermal conductivity as a function of modulation frequency that does not include any additional resistances or nonequilibrium ballistic phenomena driven by interface.

The 1/e thermal penetration depth (L_z) was determined using the solution to the radially symmetric heat diffusion equation where the full spatial temperature profile was calculated.[16] The L_z of interest is that within the $Si_{80}Ge_{20}$ substrate. As such, the temperature at the substrate surface adjacent to the Al transducer was used as the reference temperature for which the 1/e decay length was determined. Because the pump radius, r_0, was very large such that for all

modulation frequencies (ω_0) used, $\omega_0 \gg \mathfrak{D}/r_0^2$, where $\mathfrak{D}$ is the thermal diffusivity of $Si_{80}Ge_{20}$, the L_z calculated was the same as that estimated using the equation

$$L_z = \sqrt{\frac{2\mathfrak{D}}{\omega_0}}$$

Koh *et al.*[17] showed that the amplitude of heat conduction at high frequencies can be approximated using an effective thermal conductivity reduced by omitting ballistic phonons with mean free paths greater than $2L_z$. In agreement with this finding, we use $2L_z$ to compare experimentally determined effective thermal conductivities of nanograined $Si_{80}Ge_{20}$ with the FBL, SBL, and DEM models presented in this work.

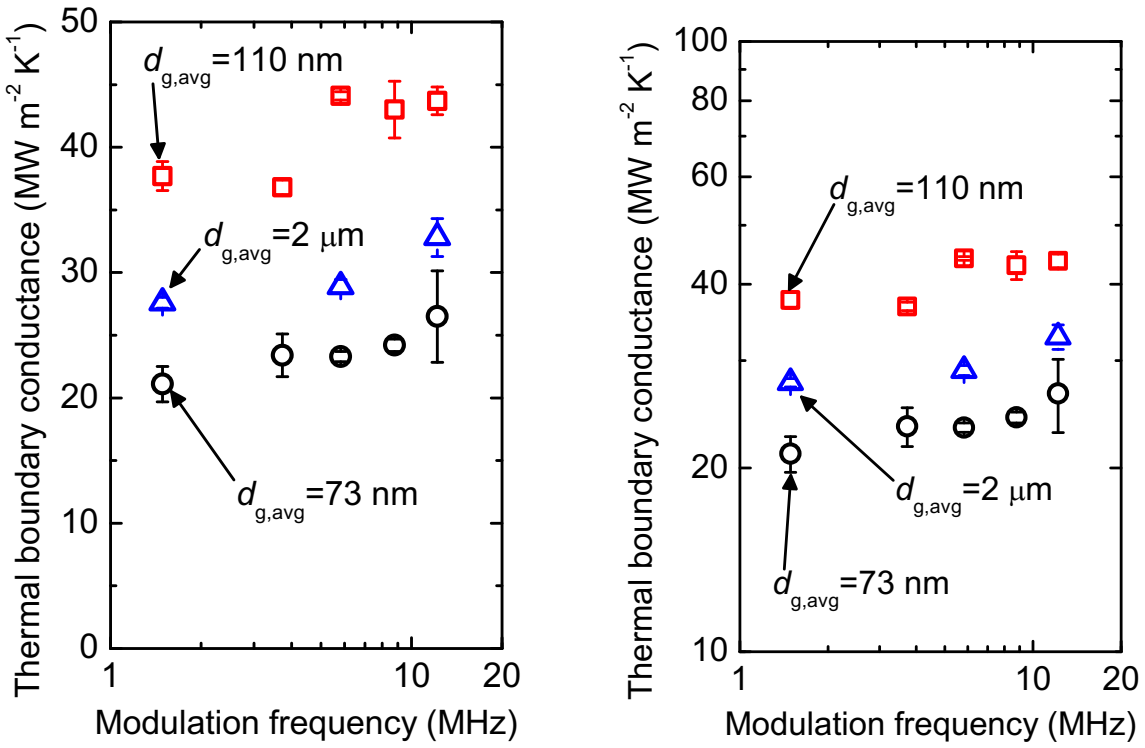

Fig. S1. Thermal boundary conductance as a function of pump modulation frequency for the three different Al/$Si_{80}Ge_{20}$ interfaces studied in this work. The average grain size, $d_{g,avg}$ of each $Si_{80}Ge_{20}$ sample is indicated in each graph. The same data is shown in each graph just plotted on a (left) semi-log scale (linear y – log x) or a (right) log-log scale (log y – log x).

S4. The cut-off mean free path vs thermal penetration depth determined by the bridge function and hard cutoff approaches

We can state equations for the low and high frequency mode heat fluxes at wavenumber q as:

$$j(q)^{LF} = \frac{3}{5}(\mathrm{MFP(q)})^2 \frac{\partial^2 j(q)^{LF}}{\partial x^2} - k(q)^{LF} \frac{\partial \mathrm{T}}{\partial \mathrm{x}} \quad \text{(S8)}$$

$$j(q)^{HF} = -k(q)^{HF} \frac{\partial \mathrm{T}}{\partial \mathrm{x}} \quad \text{(S9)}$$

Appling Eq. (4) in the main text and $\mathrm{MFP(q)} = \tau_\mathrm{q} \mathrm{v_q}$ to the equations above, we can achieve:

$$j(q)^{LF} = \frac{3}{5}(\tau_\mathrm{q} \mathrm{v_q})^2 \frac{\partial^2 j(q)^{LF}}{\partial x^2} - \left(\frac{\mathrm{D}}{(2\pi)^3} 4\pi q^2 \hbar \omega_{\mathrm{q}\lambda} \frac{\partial \mathrm{n_{q\lambda}}}{\partial \mathrm{T}}\right) \mathrm{v}_q^2 \tau_\mathrm{q} \frac{\partial \mathrm{T}}{\partial \mathrm{x}} \quad \text{(S10)}$$

$$j(q)^{HF} = -\left(\frac{\mathrm{D}}{(2\pi)^3} 4\pi q^2 \hbar \omega_{\mathrm{q}\lambda} \frac{\partial \mathrm{n_{q\lambda}}}{\partial \mathrm{T}}\right) \mathrm{v}_q^2 \tau_\mathrm{q} \frac{\partial \mathrm{T}}{\partial \mathrm{x}} \quad \text{(S11)}$$

The total heat-flux for both low frequency mode and high frequency mode contributions can be achieved by integrating $j(q)^{LF}$ and $j(q)^{HF}$ over corresponding q space. We can find the wavenumber q corresponding to cut-off MFP by varying q until the total heat-flux in the low frequency mode equals to the total heat-flux in the high frequency mode; in other words, we make the assumption in this model that $j^{LF} = j^{HF}$, which defines the cutoff wavenumber. The cut-off MFP is determined by using this cutoff wavenumber q. The normalization factor D was found to be 0.901 by equating the experimental specific heat to the calculated value, which is calculated via the expression in parenthesis in Eqs. S10 and S11.

The cut-off mean free path determined by hard cutoff equates the thermal penetration depth achieved by TDTR to the mean free path. Any phonons with mean free path larger than the measured thermal penetration depth are eliminated, and do not make any contribution to the accumulated thermal conductivity. The cut-off mean free path determined by bridge function separates the thermal conductivity of the samples into a high frequency mode component (diffusive) and low frequency mode component (quasi-ballistic). This method model equates the low and high frequency mode heat fluxes, which defines the cutoff wavenumber.

S5. Details of spectral thermal conductivity calculations using the DEM approach for nanograined $Si_{80}Ge_{20}$ systems

To achieve the spectral thermal conductivity for nanograined systems, we add $d\varphi$ of particles to the host. After each addition, the thermal conductivity of the new host $\kappa_h(\varphi)$ is updated to $\kappa\left(\frac{\varphi}{1-d\varphi}\right)$. This updated term can be expanded to:

$$\kappa\left(\frac{\varphi}{1-d\varphi}\right) = \kappa(\varphi) + \varphi d\kappa(\varphi) \quad \text{(S12)}$$

So the transformation relation can be expressed as: $\kappa_h(\varphi) \rightarrow \kappa(\varphi) + \varphi d\kappa(\varphi)$

Then we consider the phonon scattering by the added particles, the updated thermal conductivity of the host becomes:

$$\kappa_h(q,\varphi) = \frac{1}{3}C_h(q,\varphi)v_h(q,\varphi)L_{h,x}(q,\varphi+d\varphi) = \frac{1}{3}C_h(q,\varphi)v_h(q,\varphi)^2(A(\omega_q)^4 + B(\omega_q)^2T^3 + v\frac{6(\varphi+d\varphi)}{\pi a^3}(\sigma_{\text{Rayleigh}}{}^{-1} + \sigma_{\text{near geometrical}}{}^{-1})^{-1})^{-1} \quad \text{(S13)}$$

Expand the equation above and only keep the first-order terms, we can get:

$$\kappa_h(q,\varphi) = \kappa(q,\varphi)(1 - \frac{18\kappa(q,\varphi)(\sigma_{\text{Rayleigh}}{}^{-1}+\sigma_{\text{near geometrical}}{}^{-1})^{-1}}{\pi v(q,\varphi)a^3C(q,\varphi)}d\varphi) \quad \text{(S14)}$$

By writing in terms of $d\varphi$, we can achieve that

$$\kappa(q,\varphi) = \kappa_{host}(q,\varphi)(1 + \frac{3\left(\kappa_p(q)(1-\alpha(q,\varphi))-\kappa_{host}(q,\varphi)\right)}{\kappa_p(q)(1+2\alpha(q,\varphi))+2\kappa_{host}(q,\varphi)}d\varphi) \quad \text{(S15)}$$

In addition, we have

$$\kappa(q,\varphi+d\varphi) = \kappa(q,\varphi) + d\kappa(q,\varphi) \quad \text{(S16)}$$

Combining (4) and (5), we can achieve that when φ is approaching 1:

$$\kappa(q) = \frac{\kappa_p(q)}{1+\frac{\alpha_{p0}(q)*\kappa_p(q)}{\kappa_{p0}(q)}} \quad \text{(S17)}$$

$\kappa_p(q)$ is the thermal conductivity of embedded nanoparticle with wavenumber q, defined as:

$$\kappa_p(q) = \frac{1}{3}C_p(q)v_p(q)L_p(q) \quad \text{(S18)}$$

where,

$$C_p(q) = 9\frac{9N}{(q_m)^3}q^2\frac{\hbar(qv)^2}{k_\beta T^2}\frac{e^{\frac{\hbar qv}{k_\beta T}}}{(e^{\frac{\hbar qv}{k_\beta T}}-1)^2} \quad \text{(S19)}$$

$$L_p(q) = v_p(q) * \left(A(\omega_q)^4 + B{\omega_q}^2 Te^{(-c/T)} + v_s/l\right)^{-1} \quad \text{(S20)}$$

$\kappa_{p0}(q)$ is the intrinsic lattice thermal conductivity of particle material in bulk form, defined as:

$$\kappa_{p0}(q) = \frac{1}{3}C_p(q)v_p(q)L_{p0}(q) \quad \text{(S21)}$$

$$L_{p0}(q) = v_p(q) * \left(A(\omega_q)^4 + B{\omega_q}^2 Te^{(-c/T)}\right)^{-1} \quad \text{(S22)}$$

and the thermal resistance parameter $\alpha_{p0} = R_{p0}\kappa_{p0}/(d/2)$, where $R_{p0} \approx 8/(C_{p0}v_{p0})$.

Further specific details of each of the three model calculations are listed below

Fixed Boundary Length (FBL) Model:

$$\kappa_p(q) = \frac{1}{3}C_p(q)v_p(q)L_p(q)$$

$$C_p(q) = 9\frac{9N}{(q_m)^3}q^2\frac{\hbar(qv)^2}{k_\beta T^2}\frac{e^{\frac{\hbar qv}{k_\beta T}}}{(e^{\frac{\hbar qv}{k_\beta T}}-1)^2}$$

$$L_p(q) = v_p(q) * \left(A(\omega_q)^4 + B{\omega_q}^2 Te^{(-c/T)} + v_s/L\right)^{-1}$$

L is the particle size.

Spectral Boundary Length Model:

$$\kappa_p(q) = \frac{1}{3}C_p(q)v_p(q)L_p(q)$$

$$C_p(q) = 9\frac{9N}{(q_m)^3}q^2\frac{\hbar(qv)^2}{k_\beta T^2}\frac{e^{\frac{\hbar qv}{k_\beta T}}}{(e^{\frac{\hbar qv}{k_\beta T}}-1)^2}$$

$$L_p(q) = v_p(q) * \left(A(\omega_q)^4 + B{\omega_q}^2 Te^{(-c/T)} + v_s/l\right)^{-1}$$

where l is the length characteristic, defined as $l = (\rho * \sigma)^{-1}$, and is frequency dependent.

$$\sigma_{Ray} = \pi R^2 \chi^4 \left(\frac{\beta^2}{4} \left(\frac{\Delta M}{M} \right)^2 + 3\beta^8 \left(\frac{\Delta K}{K} \right)^2 \frac{(\sin \frac{\beta |\vec{q}| \delta}{2})^4}{\left(\frac{\beta |\vec{q}| \delta}{2} \right)^4} \right) \frac{\pi(\cos(4\chi) - 1 + (4\chi)\sin(4\chi) + 32\chi^4 - 8\chi^2)}{16\chi^6}$$

$$\sigma_{nGeo} = 2\pi R^2 (1 - \frac{\sin\left(2\chi\left(\frac{q'}{q} - 1\right)\right)}{\chi\left(\frac{q'}{q} - 1\right)} + \frac{(\sin\left(\chi\left(\frac{q'}{q} - 1\right)\right))^2}{(\chi\left(\frac{q'}{q} - 1\right))^2})$$

Differential Effective Medium (DEM) Model:

$$\kappa(q) = \frac{\kappa_p(q)}{1 + \frac{\alpha_{p0}(q) * \kappa_p(q)}{\kappa_{p0}(q)}}$$

where $\kappa_p(q) = \frac{1}{3} C_p(q) v_p(q) L_p(q)$

$$C_p(q) = 9 \frac{9N}{(q_m)^3} q^2 \frac{\hbar (qv)^2}{k_\beta T^2} \frac{e^{\frac{\hbar qv}{k_\beta T}}}{(e^{\frac{\hbar qv}{k_\beta T}} - 1)^2}$$

$$L_p(q) = v_p(q) * \left(A\left(\omega_q\right)^4 + B{\omega_q}^2 T e^{(-c/T)} + v_s/l \right)^{-1}$$

$\kappa_{p0}(q)$ is the intrinsic lattice thermal conductivity of particle material in bulk form, defined as:

$$\kappa_{p0}(q) = \frac{1}{3} C_p(q) v_p(q) L_{p0}(q)$$

$$L_{p0}(q) = v_p(q) * \left(A\left(\omega_q\right)^4 + B{\omega_q}^2 T e^{(-c/T)} \right)^{-1}$$

and the thermal resistance parameter $\alpha_{p0} = R_{p0} \kappa_{p0} / (d/2)$, where $R_{p0} \approx 8/(C_{p0} v_{p0})$.

Acknowledgment

This material is based upon work supported by the Air Force Office of Scientific Research under Award No. FA9550-15-1-0079.

References for Supplemental Material

1. Z. Wang and N. Mingo, "Diameter dependence of SiGe nanowire thermal conductivity," *Applied Physics Letters* **97**, 101903 (2010).
2. R. Cheaito, J. C. Duda, T. E. Beechem, K. Hattar, J. F. Ihlefeld, D. L. Medlin, M. A. Rodriguez, M. J. Campion, E. S. Piekos and P. E. Hopkins, "Experimental Investigation of Size Effects on the Thermal Conductivity of Silicon-Germanium Alloy Thin Films," *Physical Review Letters* **109**, 195901 (2012).
3. W. Kim and A. Majumdar, "Phonon scattering cross section of polydispersed spherical nanoparticles," *Journal of Applied Physics* **99**, 084306 (2006).
4. D. Wu, A. S. Petersen and S. J. Poon, "Effective scattering cross-section in lattice thermal conductivity calculation with differential effective medium method," *AIP Advances* **3**, 082116 (2013).
5. D. G. Cahill, "Analysis of heat flow in layered structures for time-domain thermoreflectance," *Review of Scientific Instruments* **75**, 5119-5122 (2004).
6. P. E. Hopkins, "Thermal transport across solid interfaces with nanoscale imperfections: Effects of roughness, disorder, dislocations, and bonding on thermal boundary conductance," *ISRN Mechanical Engineering* **2013**, 682586 (2013).
7. A. J. Schmidt, "Pump-probe thermoreflectance," *Annual Review of Heat Transfer* **16**, 159-181 (2013).
8. P. E. Hopkins, J. R. Serrano, L. M. Phinney, S. P. Kearney, T. W. Grasser and C. T. Harris, "Criteria for cross-plane dominated thermal transport in multilayer thin film systems during modulated laser heating," *Journal of Heat Transfer* **132**, 081302 (2010).
9. C. Y. Ho, R. W. Powell and P. E. Liley, "Thermal conductivity of the elements," *Journal of Physical and Chemical Reference Data* **1**, 279-422 (1972).
10. M. W. J. Chase, "NIST-JANAF Thermochemical Tables, Fourth Edition," *Journal of Physical and Chemical Reference Data Monographs or Supplements* **9**, 1-1951 (1998).
11. R. B. Wilson and D. G. Cahill, "Limits to Fourier theory in high thermal conductivity single crystals," *Applied Physics Letters* **107**, 203112 (2015).
12. R. B. Wilson and D. G. Cahill, "Anisotropic failure of Fourier theory in time-domain thermoreflectance experiments," *Nature Communications* **5**, 5075 (2014).
13. B. Abeles, "Lattice thermal conductivity of disordered semiconductor alloys at high temperatures," *Physical Review* **131**, 1906-1911 (1963).
14. Y. K. Koh and D. G. Cahill, "Frequency dependence of the thermal conductivity of semiconductor alloys," *Physical Review B* **76**, 075207 (2007).
15. P. G. Klemens, "The scattering of low-frequency lattice waves by static imperfections," *Proceedings of the Physical Society of London. Section A* **68**, 1113-1128 (1955).
16. J. L. Braun and P. E. Hopkins, "Upper limit to the thermal penetration depth during modulated heating of multilayer thin films with pulsed and continuous wave lasers: A numerical study," *Journal of Applied Physics* **121**, 175107 (2017).
17. Y. K. Koh, D. G. Cahill and B. Sun, "Nonlocal theory for heat transport at high frequencies," *Physical Review B* **90**, 205412 (2014).